Multidimensional Quantum Dynamical Study of β-Hydrogen Transfer in a Cationic Rhodium Complex

Maik Bittner,[†] Horst Köppel,*[,†] and Fabien Gatti[‡]

Theoretische Chemie, Physikalisch-Chemisches Institut, Universität Heidelberg, Im Neuenheimer Feld 229, 69120 Heidelberg, Germany, LSDSMS (UMR 5636-CNRS), Institut Gérhardt, CC 014, Université Montpellier II, 34095 Montpellier, Cedex 05, France

Received: October 20, 2006; In Final Form: January 4, 2007

The dynamics of migratory insertion and β-hydrogen elimination in the cationic complex $[CpRh(PH_3)H(C_2H_4)]^+$ is studied from a quantal point of view. On the basis of DFT results for the relevant stationary points of the potential energy surface, three coordinates are identified that vary strongly during the reaction. A suitable three-dimensional grid, along with an appropriate kinetic energy operator, are constructed that are employed in the subsequent wave packet propagations. The latter are performed in the spirit of transition state spectroscopy and start from the various saddle points of the potential energy surface. Vibrational periods and lifetimes for these elementary processes, relevant to homogeneous catalysis, are obtained in this way for the first time. This work is considered to provide the basis for a subsequent treatment of equilibrium rate constants and to shed new light on the electronic factors governing these prototypical reaction steps.

1. Introduction

So-called migratory insertion of an olefin into a metal−hydrogen bond and its microscopic reverse, the hydrogen elimination, are of primary importance to many catalytic reaction cycles involving transition metal complexes. They are considered elementary reaction steps relevant to hydrogenation, hydroformylation, and olefin polymerization, to mention just a few. Often an agostic intermediate exists where the insertion process is not complete and the migrating hydrogen atom is still interacting with the metal atom of the complex.[1−4] See Figure 1 for a schematic overview where spectator ligands are suppressed and the olefin is taken to be ethylene.

Theoretical treatments of these reaction steps usually confine attention to the energetics and the structural parameters of the various stationary points of the pertinent potential energy hypersurface.[5−12] These are obviously key quantities, for example, for the equilibrium rate constants within transition state theory (TST). Classical dynamical (MD) simulations of some of these reaction steps have also been reported in the literature.[13,14] Nevertheless, there are situations where a quantal treatment of the nuclear motion is required, and effects of tunneling and zero-point energy play a role that is beyond a classical description. Quantal schemes have also been developed to account for barrier-recrossing effects and thus go beyond the basic assumptions of TST.[15,16]

We have recently undertaken a first quantum dynamical study of migratory insertion and hydrogen elimination in a representative transition metal complex, the cationic complex $[CpRh(PH_3)H(C_2H_4)]^+$.[17] The choice of a late transition metal was motivated by recent work of Brookhart et al. who have developed a novel type of olefin polymerization catalysts based on late transition metals.[1−3] With these catalysts highly branched and hyperbranched polymers with interesting technical properties are obtained due to the fast β-hydrogen elimination and reinsertion on the late transition metal center. Experimental studies of the kinetics of migratory insertion in $[(C_5R_5)M(PR'_3)(H)(C_2H_4)]^+$ (R = H, Me; R′ = Me, OMe; M = Co, Rh) have appeared. Because our investigation was the first of its kind, it was preceded by a rather detailed study of the proper electronic structure method to be chosen; consequently, the dynamical study itself remained at a rather elementary stage, namely, a one-dimensional investigation along the intrinsic reaction coordinate (IRC).[18−21]

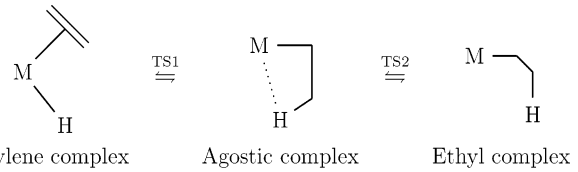

Figure 1. Schematic representation of migratory insertion (from left to right) and β-elimination (from right to left), together with the agostic intermediate.

It is the purpose of the present study to go beyond this simple picture and treat the quantum dynamics at a much more accurate level. To this end, we first have to identify a set of relevant coordinates that does not suffer from the inherent limitations of the IRC concept. This is achieved by screening the relevant stationary points of the potential energy surface and establishing a suitable set of Jacobi (or Jacobi-type) coordinates where the kinetic energy operator takes a simple, yet correct appearance. As an important byproduct, we find that a rather small subset of 3−4 vibrational degrees of freedom suffices in that description. This first step is followed by a computation of a potential energy surface of acceptable accuracy at the DFT level and, further, by the derivation of a kinetic energy operator in the curvilinear coordinates in question. In the remaining key step, we perform the necessary quantum dynamical (wave packet

* To whom correspondence should be addressed. E-mail: horst.koeppel@pci.uni-heidelberg.de. Telephone: +49 (6221) 54 52 14, Fax: +49 (6221) 54 52 21.

† Theoretische Chemie, Physikalisch-Chemisches Institut, Universität Heidelberg.

‡ LSDSMS (UMR 5636-CNRS), Institut Gérhardt, CC 014, Université Montpellier II.

10.1021/jp0668955 CCC: $37.00
Published on Web 03/06/2007

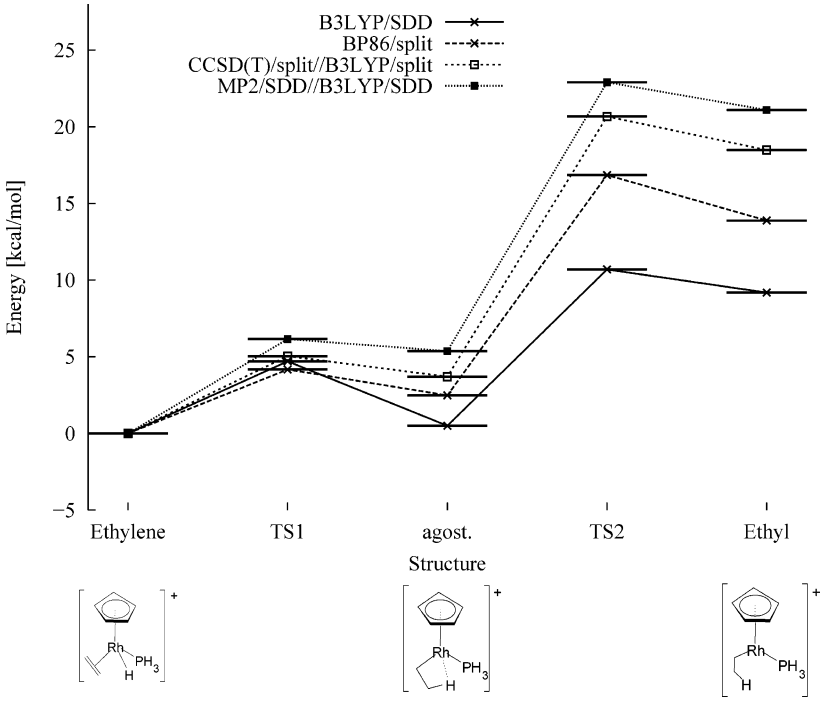

Figure 2. Stationary points of the β-hydrogen elimination/insertion process calculated with different methods/basis sets, cf. ref 17.

propagation) simulations to extract the real-time behavior of the system.[22−25] This is done not for a thermal rate problem but for a Franck−Condon transition to the transition states of the system, much in the spirit of transition-state spectroscopy.[26−29] Apart from spectra, also vibrational periods and lifetimes are obtained, not only for broad-band excitation but also for the metastable vibrational states of the agostic complex (some of the latter wave functions are also mapped out). The relevance of these findings for future experimental and theoretical investigations is pointed out at the end of this paper.

2. Electronic Structure Calculations

In our earlier work,[17] we showed that the β-hydrogen elimination/insertion involves five stationary points: the ethylene structure, which is the global minimum of the potential energy surface (PES), the agostic structure, which lies 2.4 kcal/mol higher, the ethyl structure, which is the highest local minimum (13.9 kcal/mol), and the interconnecting transition states TS1 (4.2 kcal/mol) and TS2 (16.8 kcal/mol) (see Figure 2). In this study, we tested density functional methods (B3LYP[30,31] and BP86[32,33]) and perturbation theory methods (MP2−MP4)[34−36] by comparing with coupled cluster calculations including triple excitations [CCSD(T)].[37−39]

For the electronic structure calculations, the Gaussian 03 software package has been used.[40] A combined basis set was used for the ab initio calculations: we used standard SDD[41] together with the 6-31G** basis set.[42−44] Our approach was to improve the description of the "active" hydrogen atoms by additional p-functions. The active hydrogen atoms are the terminal hydrogen atoms at the β-carbon in the ethylene moiety and the migrating hydrogen atom. The transition metal was treated with the SDD, active hydrogens, phosphorus, and carbon were treated with the 6-31G** basis set, and the nonactive hydrogen atoms were treated with 6-31G* (only s -functions). The reliability of this compromise has been proven earlier.[17] We call this the *split* basis. [It corresponds to *split2* of our earlier work.[17]]

The energetics of the stationary points calculated with the different methods and basis sets are depicted in Figure 2. A detailed comparison of methods and basis sets is given in Table 3 of ref 17. The BP86 results lie close to the CCSD(T) numbers with typical deviations of the energies of the most important stationary points (TS1 and agostic structure) of 0.7 kcal/mol (see Figure 2, and also Table 3 of ref 17). The BP86 results are more accurate and the method is also slightly faster than B3LYP (factor 1.1). From this result and the comparison of the geometries, we conclude that BP86 with the split basis describes the energies and the geometric parameters of the stationary points rather accurately and that it is fast enough to generate a PES. It will be used below for the wave packet propagations. The energies given in the first paragraph above are calculated with this method.

For the stationary points, we screened many geometric parameters, as shown in Figure 3, to determine the reactive coordinates for which the PES has to be calculated. The geometries of the stationary points are already described in our earlier work.[17] The variables R_1 and R_2 define the H−H distances at the two different carbon atoms in the ethylene moiety. R_{CC}, R, R_H, θ, and γ are depicted in Figure 4. The angles θ_3 and θ_4 describe the angles between the C−C bond in ethylene and the vector that connects a carbon atom with the center of mass of a H−H subsystem. ϕ is the out-of-plane dihedral angle of ethylene with respect to the plane defined by the three reactive centers X−Rh−H (see Figure 4). The angles θ and γ represent so-called Jacobi angles, which are more advantageous for later purposes than the more familiar bond angles α and β. Their use will be further detailed in Section 3.

From Figure 3, we conclude that the insertion/elimination reaction involves three major reaction coordinates: θ, γ, and R_H (full lines). These coordinates are changing most strongly, while the others remain approximately constant. As a first step, we assume here that the reactive centers remain planar ($\phi \approx \pi$). Looking now at the ethylene structure, Figure 5, one sees that it is mapped on the coordinate system of Figure 4, which defines the kinetic energy operator, eq 1 below.

From the range of the three relevant coordinates (θ, γ, R_H) we are able to define the range for the ab initio scan to generate the PES. The coordinate range of the raw potential energy

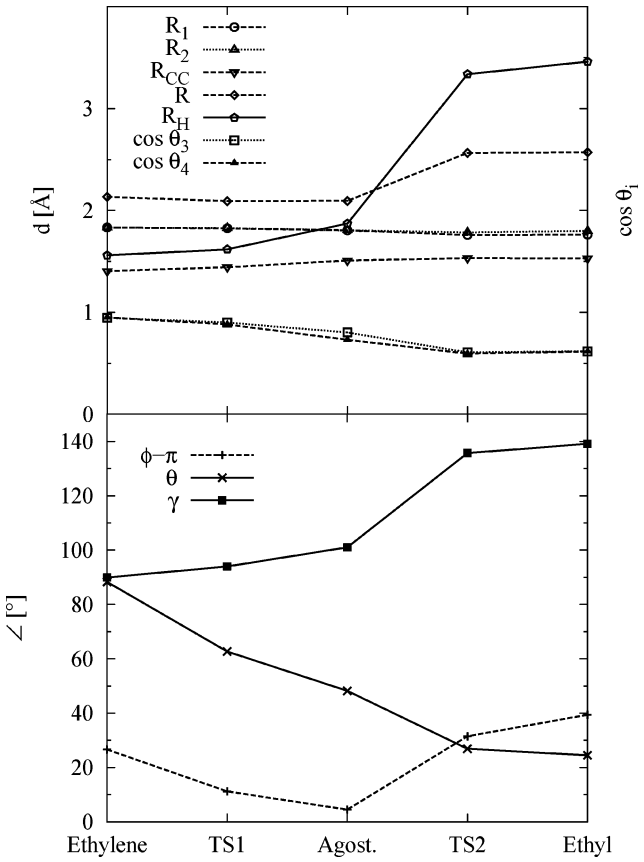

Figure 3. Variation of the coordinates for the different stationary points (B3LYP/SDD).

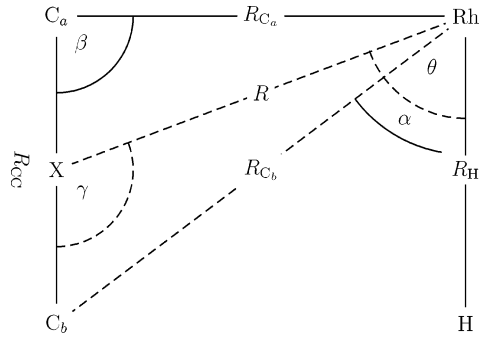

Figure 4. Inner and Jacobi coordinates for the kinetic energy operator for the four reactive centers which prove to be important for this study.

surface is given in Table 2. The table gives a total number of 2583 ab initio points. At the edges of the grid, some points have not been converged. Therefore, we calculated additional points in the region of TS1. In total, the surface includes 2669 ab initio points, which are inter- and extrapolated with an additional Mathematica package.[45] The package provides a flexible fitting function for the potential, which can be evaluated at any arbitrary position. The order and range of a local polynomial fitting function must be specified. If the range is short, the function just interpolates. If the range is long, the function behaves like a least-squares polynomial fitting function. Order and range are optimized to get a smooth and accurate energy surface compared to the original ab initio data points. The resulting fitting error is 0.17 kcal/mol for TS1 and 0.96 kcal/mol for the agostic structure.

The PES thus generated based on the BP86/split2 data is shown in Figure 6. The pictures of the PES show the position of the fully optimized stationary points as black dots and the scanned reaction path as a full black line through these points.

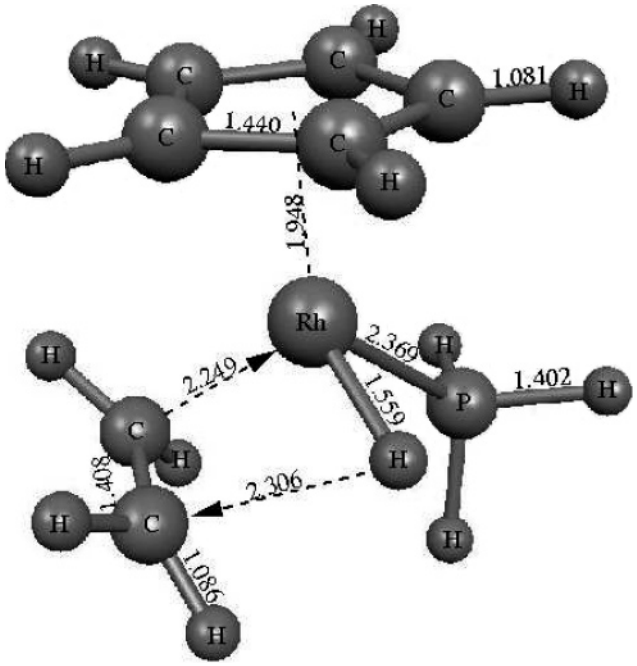

Figure 5. Ethylene complex, the global minimum on the PES (0.0 kcal/mol).[17] Distances in Å, B3LYP/SDD.

TABLE 1: Constants Employed in the Operator of the Kinetic Energy (in Å)[a]

R	R_{CC}	R_H
2.072	1.442	1.620

[a] R_H is constant only in the 2D calculation

TABLE 2: Coordinate Grid Employed for the Ab Initio Calculation of the PES

	min	max	Δ
α [deg]	15.0	75.0	10.0
β [deg]	50.0	130.0	10.0
R_H [Å]	1.5	3.5	0.05

The reaction path results from a scan along the angles α and β where the other coordinates are always relaxed. This path is discussed in detail in our previous 1D calculations.[17] For the stationary points we have different R_H bond lengths. For the ethylene structure we find $R_H = 1.565$ Å, for TS1 $R_H = 1.620$ Å, for the agostic structure $R_H = 1.782$ Å, and for the ethyl structure $R_H = 3.423$ Å. The top panel of Figure 6 refers to $R_H = 1.565$ Å (for convenience, we call this PES *ethylene PES*), the minimum of this cut is located at the coordinates of the fully optimized ethylene minimum. This global 2D minimum is moving along the path if one increases R_H. The PES with $R_H = 1.620$ Å is called analogously *TS1 PES* below. For $R_H = 1.782$ Å (*agostic PES*), the global 2D minimum is at the coordinates of the agostic structure. For $R_H = 3.423$ Å (*ethyl PES*), the minimum is found at the coordinates of the ethyl minimum. Middle and lower panels of Figure 6 show the agostic and the ethyl PES. The 3D PES is a composition of those cuts and all data points in between.

3. Quantum Dynamical Methods

3.1. Operator of the Kinetic Energy. The inspection of the geometric parameters of the stationary points has shown that the β-hydrogen elimination/insertion involves three essential coordinates and four atomic centers, as depicted in Figure 4. (The four centers are those atoms between which bonds are broken or created during the reaction.) The figure also shows

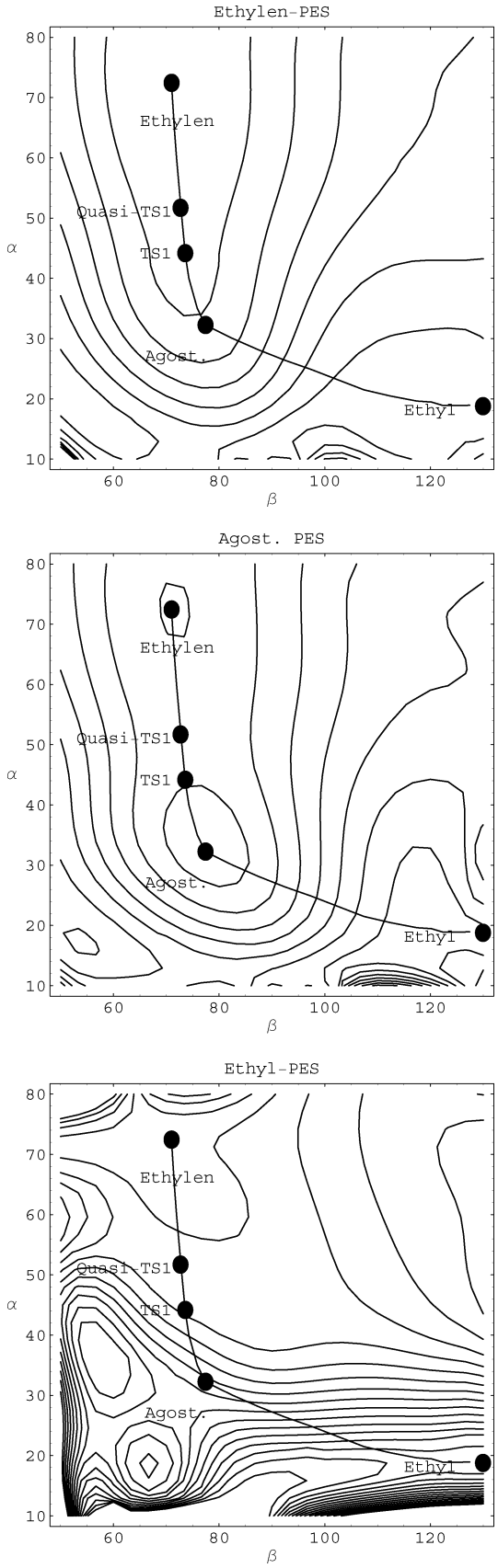

Figure 6. Potential energy surface in inner coordinates for different R_H (BP86/split2). Angles in deg, R_H in Å.

the relation between the inner coordinates (α, β, R_H) and the Jacobi coordinates (θ, γ, R_H) involved.[46,47] Jacobi coordinates refer to the centers of mass between suitable subsystems (here diatomics), while inner coordinates refer to nuclei and bonds. Here, we consider the special case that the center of mass of the Rh−H subsystem is located approximately at the transition metal atom Rh. As pointed out in the previous section during the isomerization reaction, the four reactive centers retain an approximately planar configuration ($\phi \approx \pi$). A good first approach for the kinetic energy is therefore obtained by eliminating the terms involving $\partial/\partial\varphi$ in the well-known diatom−diatom operator (see, for example, refs 48, 49). The angle φ is the spherical coordinate of $\overrightarrow{RhH}$ (Appendix A). After this elimination the operator of the kinetic energy reads:

$$\mathcal{T} = -\frac{\hbar^2}{2}\left(\frac{1}{\mu_H R_H^2} + \frac{1}{\mu_R R^2}\right)\frac{\partial^2}{\partial\theta^2} - \frac{\hbar^2}{2}\left(\frac{1}{\mu_{CC} R_{CC}^2} + \frac{1}{\mu_R R^2}\right)\frac{\partial^2}{\partial\gamma^2} - \frac{\hbar^2}{\mu_R R^2 \partial\theta\partial\gamma} - \frac{\hbar^2}{2\mu_H}\frac{\partial^2}{\partial R_H^2} \quad (1)$$

The operator has the volume element $dV = d\theta\, d\gamma\, dR_H$ and the reduced masses:

$$\mu_H = \frac{m_{Rh} \cdot m_H}{m_{Rh} + m_H} \approx m_H \quad (2a)$$

$$\mu_R = \frac{m_{RhH} \cdot m_{C_2H_4}}{m_{RhH} + m_{C_2H_4}} \quad (2b)$$

$$\mu_{CC} = \frac{m_{CH_2}}{2} \quad (2c)$$

[Given our choice for the coordinate R_{CC}, an effective mass $\mu'_{CC} = m_C/2$ should be used instead of eq 2c. The effective mass in this equation implies the use of the distance between the two CH_2 centers of mass instead. Depending on the two possible choices, the error made above amounts from −10% to +17%, respectively. Equation 2c is considered a reasonable compromise between the two possible choices.] Because of only small contributions to the total operator, an extra potential term is neglected. Some distances are kept constant according to Table 1. As will be explained below, the values correspond to the geometric parameters of the first transition state (TS1). Note that R_H is kept constant only in the two-dimensional (2D) calculations. This operator can be derived from more general considerations based on dividing the whole molecule successively into smaller subsystems. The centers of mass of the two subsystems are connected by a vector that is parametrized by its length and Euler angles. The nonreactive part of each subdivision is neglected iteratively. This procedure is developed in more detail in Appendix A, which also points toward extensions by including more degrees of freedom in possible future work.

3.2. Wave Packet Propagation. To describe the nuclear motion of the β-elimination and insertion process quantum-mechanically, we solve the time-dependent Schrödinger equation explicitly.[22−25] This solution is obtained by the Lanczos−Arnoldi algorithm,[50,51] which builds up a tridiagonal matrix that has approximately the same eigenvalues as the full Hamiltonian. The solution of the time-dependent Schrödinger equation is then reduced to the diagonalization of this matrix. The Lanczos−Arnoldi algorithm is a variant of the Lanczos algorithm suitable for non-hermitian operators. We need this feature to be able to incorporate a complex absorbing potential (CAP) into the potential to simulate the decay of the complex once the wave packet reaches certain grid boundaries (see next paragraph). The potential and the wave function are represented on a 3D grid;[52,53]

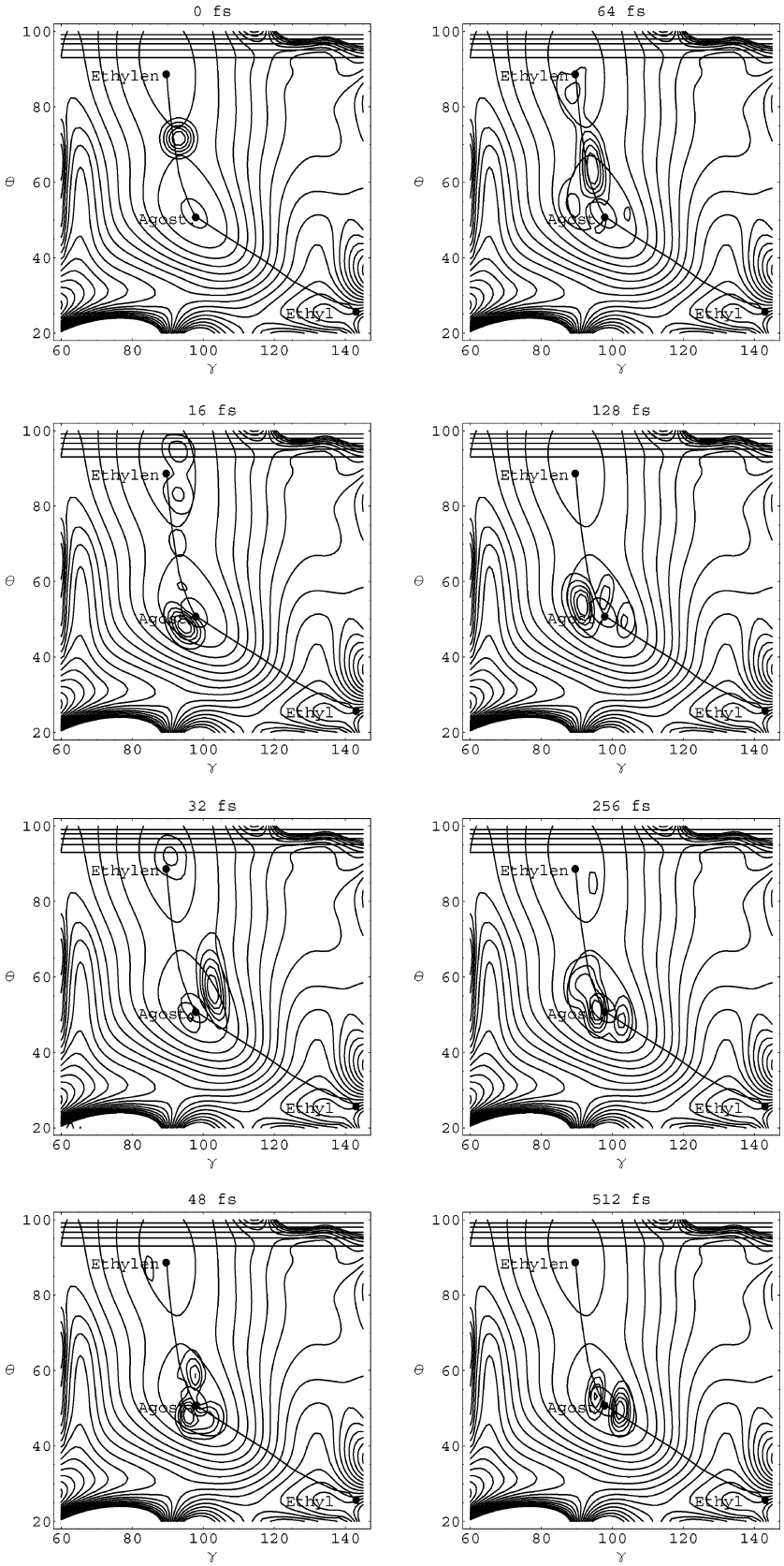

Figure 7. Snapshots of the 2D time evolution of a wave packet started at quasi-TS1 of the agostic PES. Angles in radians.

to calculate the second derivative with respect to the coordinates, the fast Fourier transformation method (FFT)[54−56] has been used.

If the catalyst isomerizes into the ethylene structure, ethylene can dissociate from the metal center, e.g., through a solvent. Ethylene will not easily reinsert; it is thus lost for the polymerization reaction. We simulate this decay process by absorbing the corresponding parts of the wave function by a CAP,[57−60] thus also preventing artificial reflections of the wave packet from the grid boundaries. This is a well-known technique in quantum dynamical treatments of reactive scattering

processes. The CAP closes the potential on one side. It has the form

$$V_{\mathrm{CAP}}(\theta) = -i\eta(\theta - \theta_0)^2 \qquad \text{for } \theta \geq \theta_0 \tag{3}$$

where η is the strength parameter of the CAP. $\theta \geq \theta_0 = 92°$ is the area "beyond" the ethylene structure.

We adjusted the CAP parameter η so that the outgoing wave packet is not reflected or transmitted. This can be controlled by observing key numbers: we monitored the energy of two prominent states, the ground state and the third excited state, the lifetime of this state, and the total norm of the wave packet after 512 fs of propagation as a function of the CAP parameter η . We find stationary solutions for the Rh complex at $\eta = 3 \times 10^{-5}$ kcal/mol·deg^{-2}. The resulting complex part of the potential is indicated in Figure 7 at the top side as horizontal lines.

The spectra are calculated by a FFT of the overlap of the initial wave packet ψ_0 and the time developed one, $\exp(-i\mathscr{H}t/\hbar)\psi_0$ (autocorrelation function $C(t)$):

$$C(t) = \langle\psi_0|e^{-(i/\hbar)\mathscr{H}t}|\psi_0\rangle \tag{4}$$

The spectrum is thus given by[61]

$$P(E) = \frac{1}{2\pi}\int_{-\infty}^{\infty} C(t)\, e^{(i/\hbar)Et}\, \mathrm{d}t \tag{5}$$

From the non-hermitian Hamilton operator $\mathscr{H}$, one gets complex energy eigenvalues E. These are extracted with filter diagonalization techniques.[62−65] The real parts give the energies of the spectral peaks in the FFT spectrum. The imaginary parts are the lifetimes of the corresponding metastable states.

If one knows the eigenenergies of a given Hamiltonian by FFT or filter diagonalization, it is possible to calculate the eigenfunctions by Fourier transformation of the time-developed wave packet at the appropriate energies. To see this, one expands the initial wave function ψ_0 in terms of the eigenfunctions. Upon Fourier transformation, this gives a sum of δ-functions. The δ-function is nonzero at the position of the eigenfunction in question:

$$\begin{aligned}
\int_{-\infty}^{\infty} |\psi(t)\rangle\, e^{(i/\hbar)E_m t}\, \mathrm{d}t &= \int_{-\infty}^{\infty} e^{-(i/\hbar)\mathscr{H}t}|\psi(0)\rangle\, e^{(i/\hbar)E_m t}\, \mathrm{d}t \\
&= \sum_{n=0}^{\infty}\int_{-\infty}^{\infty} e^{-(i/\hbar)\mathscr{H}t}|\psi_n\rangle\langle\psi_n|\psi(0)\rangle\, e^{(i/\hbar)E_m t}\, \mathrm{d}t \\
&= \sum_{n=0}^{\infty} c_n|\psi_n\rangle \int_{-\infty}^{\infty} e^{-(i/\hbar)(E_n - E_m)t}\, \mathrm{d}t \\
&= \sum_{n=0}^{\infty} c_n|\psi_n\rangle\, \delta(E_n - E_m) \\
&\approx c_m|\psi_m\rangle\, \mathrm{sinc}[(E_n - E_m)T/\hbar]
\end{aligned} \tag{6}$$

where the coefficient c_m equals $\langle\psi_n|\psi(0)\rangle$. The sinc function is defined as $\mathrm{sinc}(x) = \sin(x)/x$, and it is relevant because of the numerically limited propagation time T . This technique is known as spectral quantization.[66,67]

3.3. Initial Wave Packet and Computational Details. The calculations simulate an experiment in which a suitable laser pulse strips off an electron from the neutral complex. By pulse shaping techniques, the complex can be excited to a transition-state geometry.[68−71] In these techniques, feedback of certain observables and evolutionary algorithms are used to optimize the shape of the laser pulse. The starting position of the initial wave packets has always been chosen at TS1 because the density of available ab initio points in the vicinity of TS1 is very high. Therefore also the quality of the fitted PES in this region is very high. Because of nonconverged ab initio points in the vicinity of TS2, the PES is not so accurate in this region, and we have, therefore, not chosen this as the initial position of the wave packet.

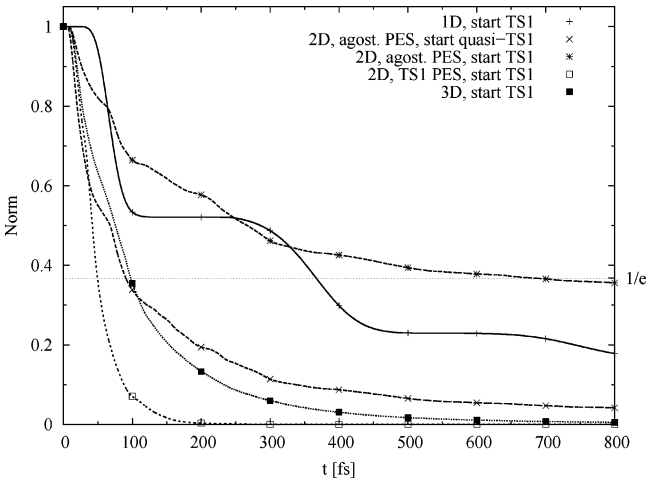

Figure 8. Time evolution of the norm of the β-hydrogen elimination/insertion process of the 1D−3D calculations.

For the key 2D calculation, "TS1" was identified visually on the agostic potential energy surface. For convenience we call it *quasi-TS1*; it is emphasized in Figure 6. The widths of the initial wave packets are chosen such that they cover approximately the peaks of the transition states. The widths are: $\Delta\theta = 4.01°$, $\Delta\gamma = 4.01°$, $\Delta R_{\mathrm{H}} = 1.15$ Å. R_{H} is used only in the 3D calculation. The wave packets have been propagated for 1024 fs with time steps of 0.05 fs and a Lanczos order of 10. The propagation grid has the dimensions $N_\theta \times N_\gamma \times N_{\mathrm{RH}} = 64 \times 64 \times 128$. The software used for the wave packet propagation was developed in our group and widely tested for the vinylidene−acetylene isomerization reaction[24] and for the β-hydrogen elimination in a 1D treatment.[17]

4. Results and Discussion

In this section, we discuss three 2D calculations on two different PES and the 3D calculation. In two dimensions, we started wave packets at TS1 and "quasi-TS1" on the agostic PES, and we started a wave packet at TS1 on the TS1 PES. Also, the 3D calculation is performed for an initial wave packet starting at TS1.

4.1. 2D Calculation. Figure 7 shows the 2D dynamics of a wave packet evolving on the agostic PES. $R_{\mathrm{H}} = 1.782$ Å corresponds here to the coordinate of the fully optimized agostic minimum. Note that the PES is given here in Jacobi coordinates (θ, γ) in contrast to Figure 6, where we showed the PES in inner coordinates (α,β). The reaction path is given in this figure by the black line, which connects the stationary points (black dots). The initial wave packet is situated at the TS1 of this surface (quasi-TS1). Now the geometry of the catalyst is mainly in a configuration close to TS1. When the packet propagates, it splits up in two parts (16 fs): One part propagates toward the ethylene minimum located near the top of the panels. For these molecules the reaction is finished. From a chemical point of view, ethylene moves away from the transition metal complex. This process is simulated by the CAP, which absorbs the part of the wave function which passes through the ethylene

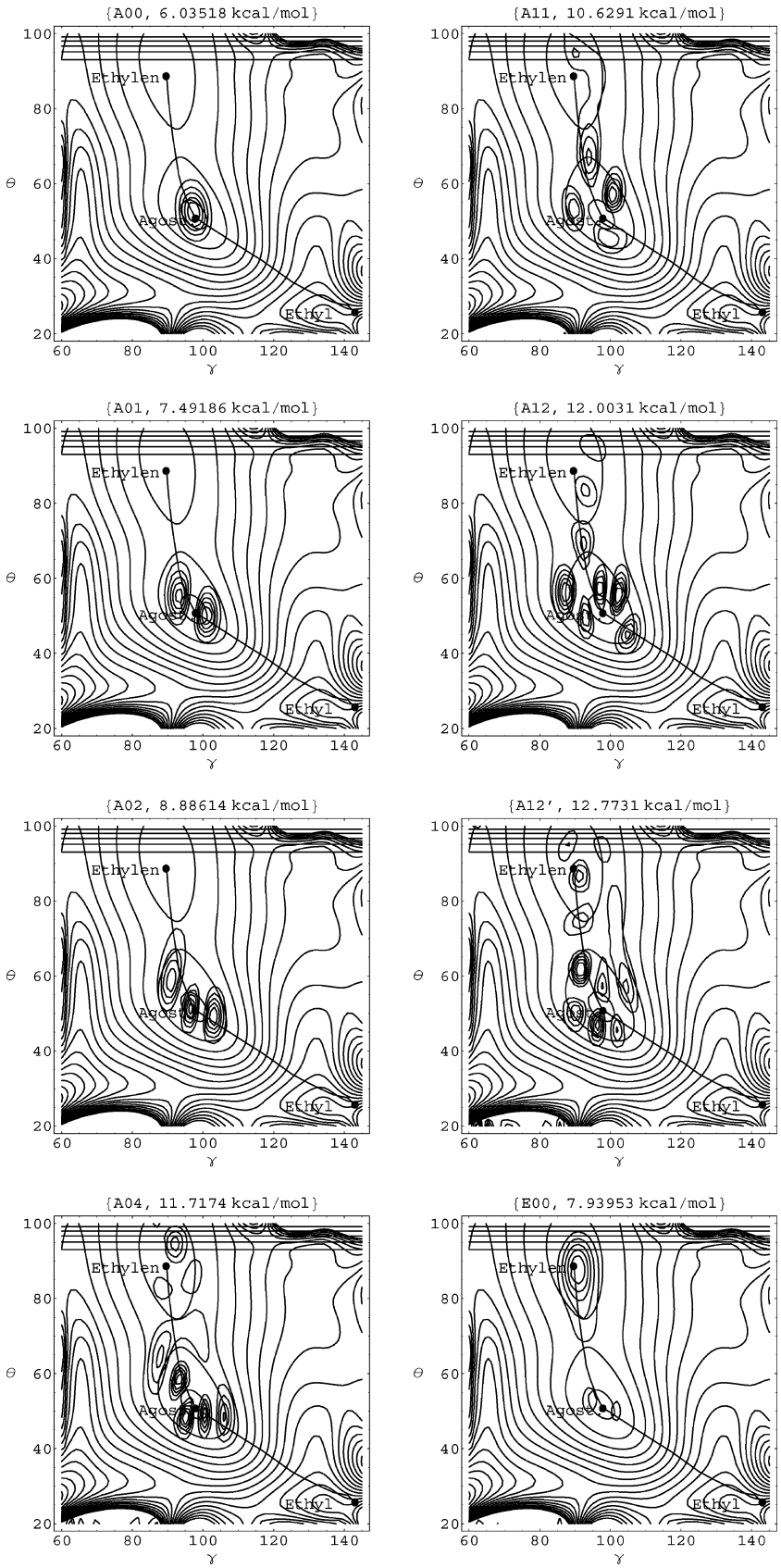

Figure 9. Eigenfunctions of the 2D calculation (agostic PES). Angles in radians.

minimum ($\theta \geq 1.547$ rad) according to eq 3. The other part of the wave packet moves into the agostic minimum, where it oscillates (see panels for 32 fs and later). The potential close to the agostic minimum can be compared with a two-dimensional harmonic potential. Each time the packet reaches TS1, a part of the packet evolves toward the ethylene minimum and will be absorbed by the CAP (eg. 16−32 fs). As times increase, more and more molecules undergo the elimination process. We

also started the wave packet on the same PES at the coordinates of the fully optimized TS1, which is closer to the agostic minimum (cf. Figure 6). Quasi-TS1 and the fully optimized TS1 do not have the same coordinates on the agostic surface because each cut through the 3D PES gives another "local" TS1. The isomerization to the ethylene species is slower because the packet is closer to the agostic minimum. On the other hand, we started the wave packet on the TS1 PES, which corresponds to $R_H = 1.620$ Å of the fully optimized TS1. This initial wave packet is placed closer to the ethylene minimum. The agostic minimum is more shallow (cf. Figure 6). We thus expect a faster isomerization. The principal oscillation in the agostic minimum and periodical absorption behavior of the wave packet is, however, the same for all initial wave functions investigated.

The stepwise absorption of the wave function can be monitored by plotting the norm of the time-dependent wave function (Figure 8). The figure summarizes the results of the earlier 1D calculation,[17] 2D calculations with different initial wave packets, and the 3D calculation (see below). We consider first the agostic PES. The norm decreases relatively slowly ($\tau \approx 660$ fs) if one places the initial wave packet at TS1. It decreases faster ($\tau \approx 90$ fs) if the initial wave packet is placed at quasi-TS1. It decreases the fastest if it is placed at TS1 of the TS1 PES ($\tau \approx 50$ fs). This behavior has been already predicted qualitatively by the discussion of the time-dependent wave function in Figure 7 and the reaction path in Figure 6.

The stepwise decrease of the norm is not as significant as for the 1D calculation,[17] but it is still visible. The 2D calculation with the initial wave packet at TS1 propagated on the TS1 PES is most similar to the 1D calculation. It is not possible to derive clear oscillation frequencies from the norm because the wave packet moves in an anharmonic 2D potential.

The eigenfunctions of the 2D calculation (agostic PES) are plotted in Figure 9. A state label and the energy of the state is plotted at the top of the panels. One can identify two different modes: one being perpendicular to the reaction path (first number of the label) and one along the reaction path (second number). A00, for example, denotes the ground state in the agostic minimum, A01 is the first excited-state of the vibration along the reaction path (it has one node), A02 is the second excited-state with vibration along the reaction path (it has two nodes), and so on. A11 is the first excited state with respect to both directions, E00 is the ground state in the ethylene minimum.

For the 2D calculation (agostic PES) and the 3D calculation (see below), the FFT spectra are plotted in Figure 10. The filter diagonalization delivers the same energies E and additionally the lifetimes τ of the states (Table 3). For the A0n series, one finds that the lifetime dramatically decreases with increasing excitation. The filter diagonalization gives intensities I, which fit well to the intensities calculated with FFT.

4.2. 3D Calculation. Figure 11 shows the time-dependent wave function resulting from the 3D calculation as a contour plot. Each point on the surfaces corresponds to a constant suitable value of the wave function ($|\psi(t)|^2 = 10^{-4}$ for all panels of the figure). This value is chosen to make all relevant features of the wave function visible at all plotted times. In the first 5 fs, the wave packet is moving in the R_H direction because of the small reduced mass μ_H in eq 2a. After 10 fs, the wave packet is concentrating in the agostic minimum. An oscillation and broadening in the agostic minimum leads to a splitting of the wave packet into two parts. One part is oscillating in the agostic minimum, while the other part is moving toward the ethylene minimum, where it is absorbed by the CAP (20 fs and later). This process is going on periodically and qualitatively the same as in the 1D[17] and 2D calculations.

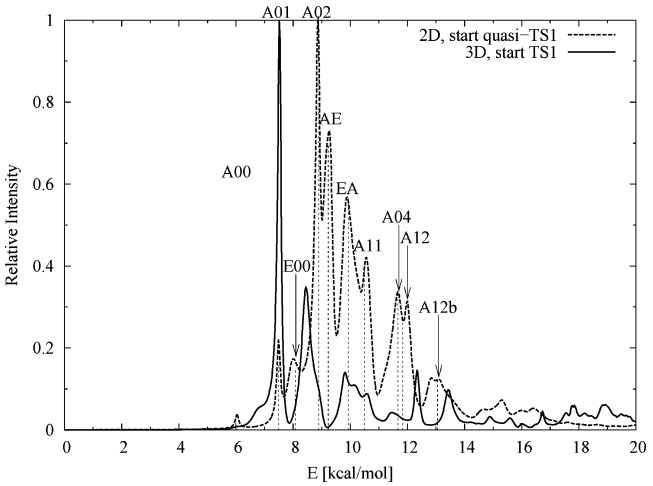

Figure 10. Spectra of the 2D and 3D calculations.

TABLE 3: Labeling, Energies *E* in kcal/mol, Intensities *I*, and Lifetimes τ (Filter Diagonalization) of the States of the 2D Calculation

min	*mn*	*E*	*I*	τ
A	00	6.035	0.03	27 ns
	01	7.492	0.12	25 ps
	02	8.886	1.00	328 fs
	04	11.717	0.37	47 fs
	11	10.629	0.58	44 fs
	12	12.003	0.21	99 fs
	12′	12.773	0.05	51 fs
E	00	7.940	0.56	45 fs
AE		9.090	0.91	74 fs
EA		9.815	0.72	40 fs

Figure 12 shows the eigenfunctions of the 3D calculation as a contour plot. The meaning of this figure is the same as in Figure 11: each point on the surface corresponds to a suitable value of $|\psi_{mnl}|^2 = 10^{-9}-10^{-7}$ depending on the figure panel. The first boxes are seen from a top view onto the $\theta-\gamma$ plane in front. Like in the 2D calculation, we have a nodal structure along the reaction path (from top left to bottom right) and a nodal structure perpendicular to the path. We denote the states as follows: the state *mnl* has the quantum number *m* perpendicular to the reaction path in the $\theta-\gamma$ plane, the quantum number *n* along the reaction path in the same plane, and the quantum number *l* perpendicular to the $\theta-\gamma$ plane. The ground state 000 (4.705 kcal/mol) is located in the agostic minimum. The nodal structure along the reaction path with three, four, and five nodes is very well visible for 030 (8.435 kcal/mol), 040 (9.011 kcal/mol), and 050 (9.794 kcal/mol). The state 140 (10.670 kcal/mol) has one nodal plane perpendicular to the reaction path and four nodal planes along it. For *mn*2 (18.758 kcal/mol), the viewpoint on the box is rotated: one looks now from the previous right-hand side onto the box (R_H is on the vertical axis, θ is on the horizontal axis). Now two nodal planes in the R_H direction are visible. Because the other structure is unclear, it is not possible to count nodes in the $\theta-\gamma$ plane.

For both dimensionalities 2D/3D, we conclude that the excitation of vibrations along the reaction path in the $\theta-\gamma$ plane is easier than excitation perpendicular to it. This is clear because a cut through the PES perpendicular to the reaction path gives

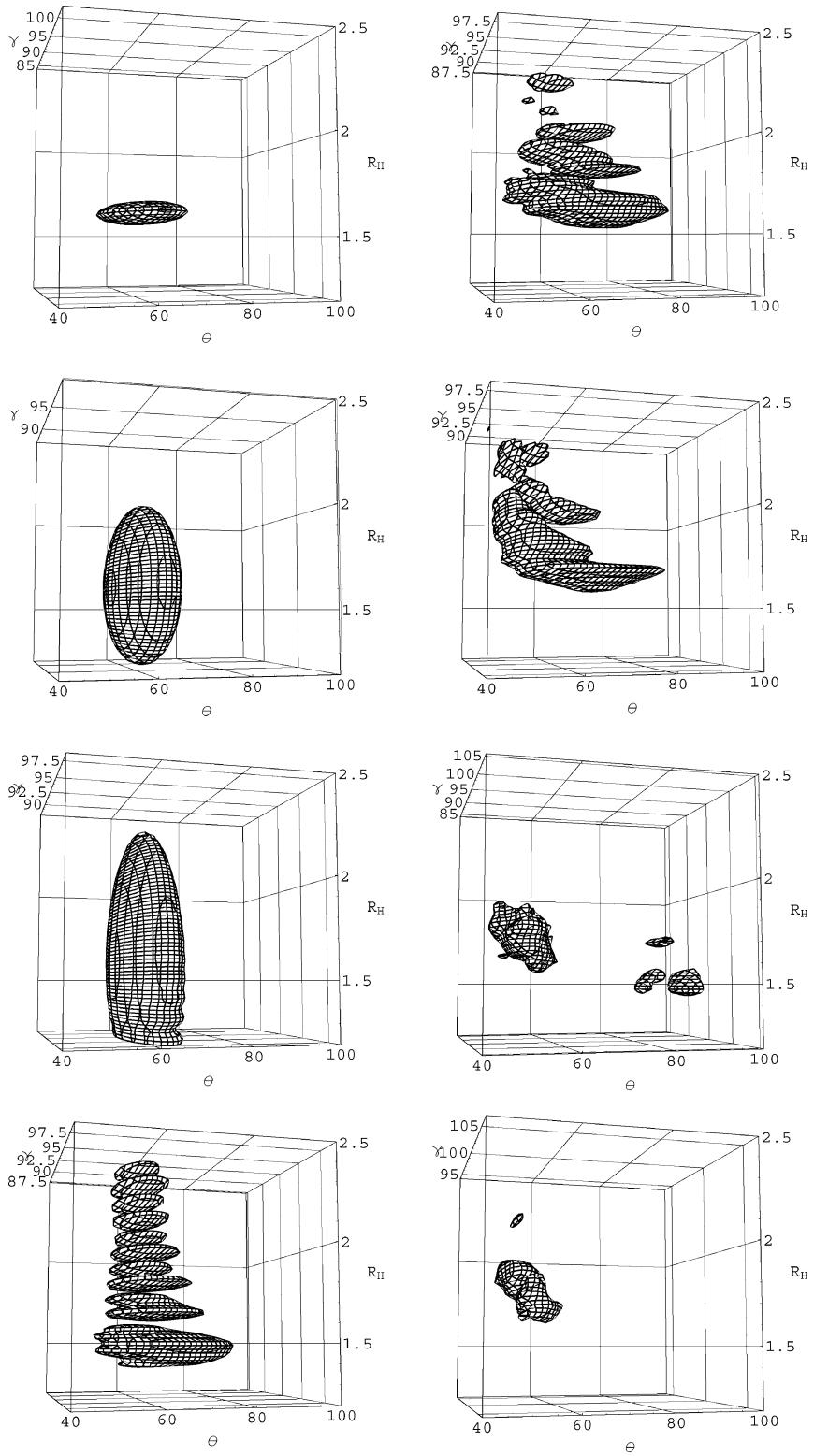

Figure 11. Snapshots of the 3D time evolution of a wave packet started at TS1 in a contour plot. Angles in radians, R_H in Å. Each point on the surfaces corresponds to a suitable constant value of $|\psi(t)|^2 = 10^{-4}$.

a narrower potential than that in the direction of the path. The latter direction is modeled by a reaction path potential already considered in ref 17.

The norm of the wave function of the 3D calculation is included in Figure 8. The norm decreases approximately as fast as in the 2D calculation, with the initial wave packet at quasi-TS1 on the agostic PES. That is the reason why we focused on this 2D calculation above. This 2D calculation models the process better than the other 2D calculations. Similar to this calculation, also for the 3D calculation we get an overall lifetime of 100 fs.

Figure 10 shows the 3D FFT spectrum (full line). The exact energies with their lifetimes are given in Table 4. In general, the spectra of the 2D and 3D calculation differ, but the ground states A00 and 000 are energetically equal. A01 and 020 have the same energy, and they describe the same vibrational direction

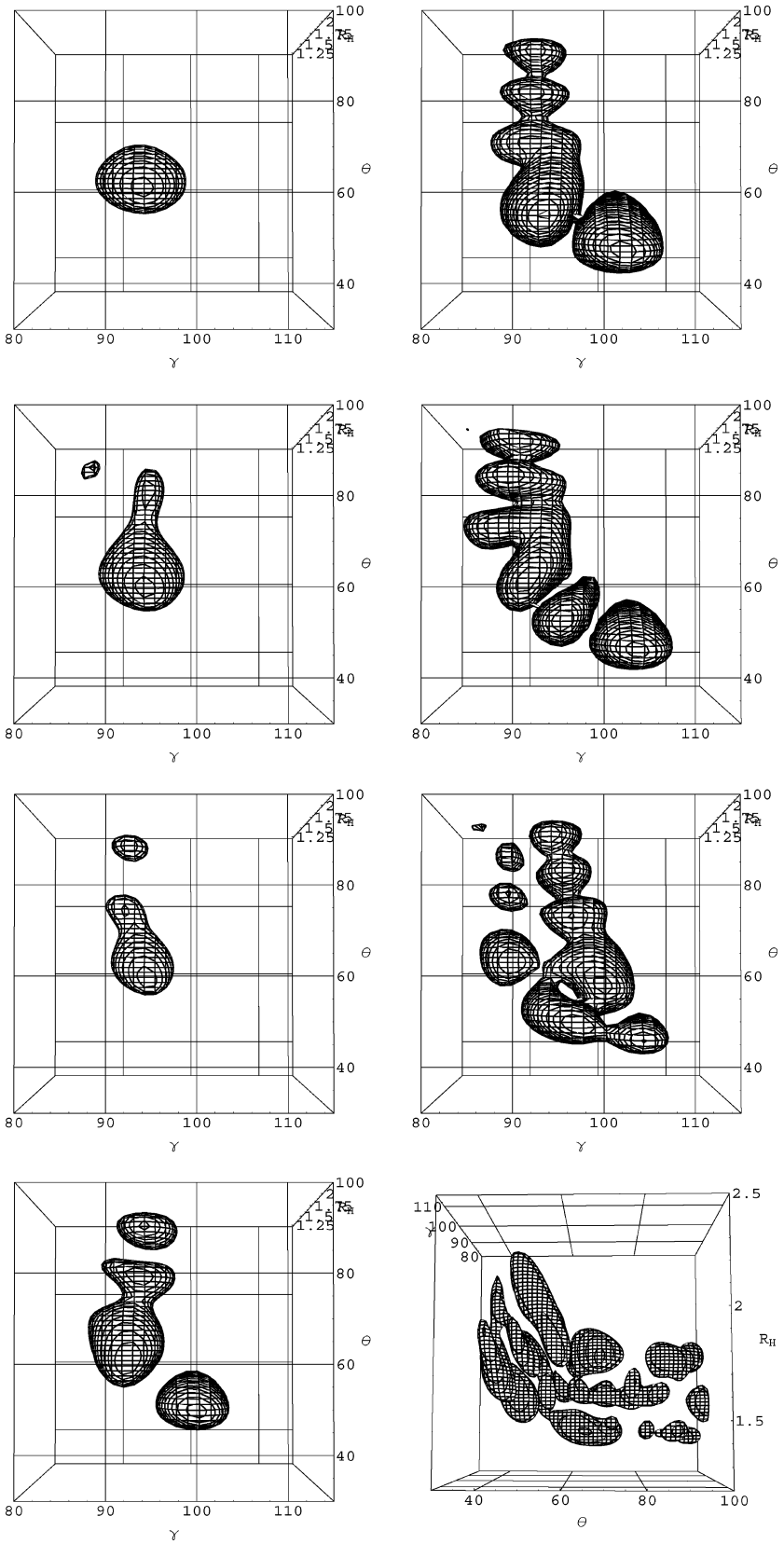

Figure 12. Eigenfunctions of the 3D calculation in a contour plot. Angles in radians, R_H in Å. Each point on the surfaces corresponds to a suitable constant value of $|\psi_{mnl}|^2 = 10^{-9}-10^{-7}$.

(along the reaction path) but different excitation. Looking at the lifetimes calculated with filter diagonalization, the states decay faster than the overall lifetime of 100 fs. We propagated the metastable wave functions directly to validate the lifetimes by inspection of the time-dependent norm. We find a very good agreement with an average deviation of only 30 fs.

5. Summary and Concluding Remarks

In this article, we have described a quantal approach to investigate the dynamics of elementary catalytic reaction steps, especially β-hydrogen elimination from an agostic transition metal complex. A reduced-dimensionality (3D) treatment could

TABLE 4: Labeling, Energies *E*, and Lifetimes τ (Filter Diagonalization) of the States of the 3D Calculation.

mnl	*E* [kcal/mol]	τ [fs]
000	4.699	44
010	5.993	42
020	6.699	26
020b	7.529	122
030	8.424	43
040	9.013	39
050	9.798	58
140	10.672	48
*mn*2	18.757	49

be set up and earlier one-dimensional calculations considerably extended in this way. Many new spectroscopic data and time constants (vibrational periods and lifetimes) were obtained, which sheds new light on the species treated and on the process in general. Further improvement of the dynamical approach would consist of including also the out-of-plane distortion mentioned in Section 2 (see Figure 3) above and possibly by including also other degrees of freedom; however, the latter would require a more approximate treatment, like a locally harmonic approximation, to save computational effort in generating the DFT potential energy surface.

As a further step in the overall line of investigation, the studies are to be extended to other ligands and transition metals to elucidate their influence on the dynamics, to consider also reinsertion processes that are suppressed in our study by the use of a complex absorbing potential, and to use these results as a basis to compute also thermal rate constants. (Remember that the present study focused on a highly nonequilibrium process, corresponding to a Franck−Condon excitation to the transition states of the system.) This is possible, e.g., by utilizing the above techniques and results within the flux−flux correlation function formalism of Miller.[15,16] In this way, it is thus ultimately hoped that these studies provide more insight into the electronic factors governing, e.g., the outcome of olefin polymerization, and thus helping in its control.

More generally, we point out the relevance of our reduced-dimensionality treatment also to other processes than those investigated here. The four atoms retained in the description are apparently just the atoms between which bonds are broken and newly formed in the chemical reaction. The present analysis established that it is mostly their structural parameters that change significantly, whereas the others remain nearly constant. If this holds true also for other systems, it might open a route to extend this line of approach to a large variety of different reactive processes, catalytic and others.

Acknowledgment. We gratefully acknowledge many helpful discussions with Hubert Wadepohl. This work has been supported financially by the Deutsche Forschungsgemeinschaft through Sonderforschungsbereich 623 "Molekulare Katalysatoren: Struktur und Funktionsdesign".

Appendix A. Derivation of the Kinetic Energy Operator

We present here a more rigorous derivation of the kinetic energy operator based on dividing the whole molecule successively into smaller subsystems. The approach rests on a polyspherical description of the molecular system.[72−75] The system is first separated into two subsystems 1 and 2. $\vec{R}_{12} = \vec{G_1G_2}$ is the Jacobi vector joining $G1$, the center of mass of the subsystem 1 ($HRhC_2H_4$), to $G2$, the center of mass of the subsystem 2 ($PH_3C_5H_5$), see Figure 13.

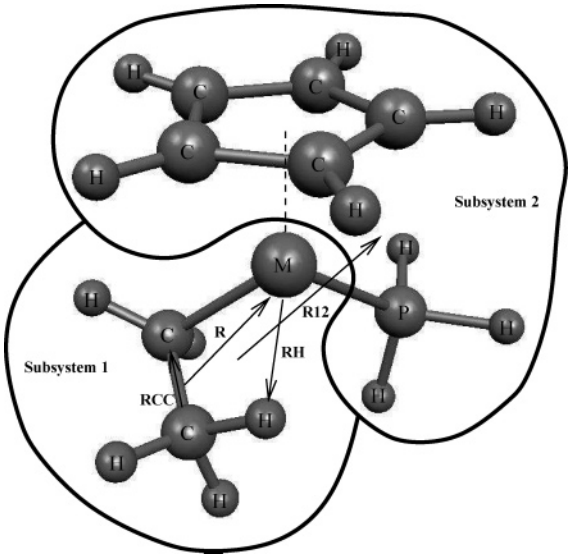

Figure 13. First division of the catalyst into two subsystems.

For the whole system ($HRhC_2H_4PH_3C_5H_5$), the exact kinetic energy operator then reads:[74,76]

$$T = T_1 + T_2 + \frac{p_{R_{12}}^2}{2\mu_{R_{12}}} + \frac{[\vec{J}^2 + (\vec{J}_1 + \vec{J}_2)^\dagger(\vec{J}_1 + \vec{J}_2) - 2\vec{J}(\vec{J}_1 + \vec{J}_2)]_{BF}}{2\mu_{R_{12}}R_{12}^2} \quad (7)$$

Here $\vec{J}$ is the total angular momentum, $\vec{J}_1$ the total angular momentum of the subsystem 1, $\vec{J}_2$ the total angular momentum of the subsystem 2, R_{12} is the length of the Jacobi vector $\vec{R}_{12}$,

$$\mu_{R_{12}} = \frac{m_{HRhC_2H_4} \cdot m_{PH_3C_5H_5}}{m_{HRhC_2H_4PH_3C_5H_5}} \quad (8)$$

T_1 is the kinetic energy of the subsystem 1, T_2 is the kinetic energy of the subsystem 2. BF denotes the Body Fixed frame defined as in refs 74 and 76 (in particular z^{BF} lies parallel to $\vec{R}_{12} = \vec{G_1G_2}$). We now only consider the case $\vec{J} = \vec{0}$. The operator
then reads:

$$T = T_1 + T_2 + \frac{p_{R_{12}}^2}{2\mu_{R_{12}}} + \frac{(\vec{J}_1 + \vec{J}_2)^\dagger(\vec{J}_1 + \vec{J}_2)_{BF}}{2\mu_{R_{12}}R_{12}^2} \quad (9)$$

In the following, we remove the parts corresponding to the subsystem 2 and $\vec{J}_1$ because the corresponding degrees of freedom change very little during the process we are interested in. Obviously, simply removing these parts makes an additional approximation. Consequently, some corrections should be added to the kinetic energy operator T_1. A comprehensive presentation of the exact derivation of rigidly or adiabatically constrained kinetic energy operators in a general context can be found elsewhere.[77−79] However, in the present paper, we deliberately neglect these corrections because the parts of the system that are frozen are much heavier than the hydrogen atom involved in the β-hydrogen elimination. In other words, we simply say that the subsystems that are frozen are infinitively heavy with respect to the hydrogen atom. Therefore, we simply have to deal with the T_1 term, which can also be separated into two

further subsystems: RhH and C_2H_4. The kinetic energy thus reads:[74,76]

$$2T_1 = 2T_{C_2H_4} + \frac{p_R^2}{\mu_R} + \frac{p_{R_H}^2}{m_{R_H}} + \frac{[\vec{L}]_{BF1}^2}{m_H R_H^2} + \frac{[\vec{J}_1^2 + (\vec{L}+\vec{J}')^\dagger(\vec{L}+\vec{J}') - 2\vec{J}_1(\vec{L}+\vec{J}')\vec{J}_1]_{BF1}}{\mu_R R^2} \quad (10)$$

where $\vec{R}$ is the Jacobi vector $\overrightarrow{GG_{RhH}}$ joining G, the center of mass of C_2H_2, to G_{RhH}, the center of mass of RhH, which can be approximated as $G_{RhH} \simeq$ Rh. BF1 is the body fixed frame of the subsystem 1 as defined in ref 74,76 (in particular z^{BF1} lies parallel to $\vec{R}$). $\vec{L}$ is the angular momentum associated with $\overrightarrow{RhH}$, and $\vec{J}'$ is the total angular momentum of C_2H_4. Moreover, we have

$$\mu_R = \frac{m_{RhH} \cdot m_{C_2H_4}}{m_{RhHC_2H_4}} \quad (11)$$

and because we work with polyspherical coordinates, the vector $\overrightarrow{RhH}$ is described by three spherical coordinates (two of them, R_H and θ, are depicted in Figure 4). Moreover, the kinetic energy operator of $T_{C_2H_4}$ could be directly derived in terms of polyspherical coordinates from the general expression given in ref 80 (see, for instance, Figure 1 in ref 80). If we freeze again the internal motion in the C_2H_2 subsystem and neglect the corresponding corrections,[77,78] we arrive at a simple diatom−diatom problem (see, for instance, the expression of the operator for a tetra-atomic system in refs 73, 75, and 81):

$$2T_1 = \frac{\vec{J}'^\dagger \vec{J}'_{BF1}}{\mu_{CC} R_{CC}^2} + \frac{p_{R_{CC}}^2}{\mu_{CC}} + \frac{p_R^2}{\mu_R} + \frac{p_{R_H}^2}{m_{R_H}} + \frac{\vec{L}_{BF1}^2}{m_H R_H^2} + \frac{[\vec{J}_1^2 + (\vec{L}+\vec{J}')^\dagger(\vec{L}+\vec{J}') - 2\vec{J}_1(\vec{L}+\vec{J}')\vec{J}_1]_{BF1}}{\mu_R R^2} \quad (12)$$

This results in the following $J_1 = 0$ kinetic energy operator in terms of the six degrees of freedom retained:

$$2T = -\frac{\hbar^2}{\mu_H}\frac{\partial^2}{\partial R_H^2} - \frac{\hbar^2}{\mu_R}\frac{\partial^2}{\partial R^2} - \frac{\hbar^2}{\mu_{CC}}\frac{\partial^2}{\partial R_{CC}^2} - \hbar^2\left(\frac{1}{m_H R_H^2} + \frac{1}{\mu_R R^2}\right)\left(\frac{1}{\sin\theta}\frac{\partial}{\partial\theta}\sin\theta\frac{\partial}{\partial\theta} + \frac{1}{\sin^2\theta}\frac{\partial^2}{\partial\varphi^2}\right) + \frac{(2p_\gamma - i\hbar\cot\gamma)i\hbar\left(-\cos\varphi\frac{\partial}{\partial\theta} + \sin\varphi\cot\theta\frac{\partial}{\partial\varphi}\right)}{\mu_R R^2} - \hbar^2\left(\frac{1}{\mu_{CC}R_{CC}^2} + \frac{1}{\mu_R R^2}\right)\left(\frac{1}{\sin\gamma}\frac{\partial}{\partial\gamma}\sin\gamma\frac{\partial}{\partial\gamma}\right) + \frac{p_\varphi^2}{\sin^2\gamma}\left(\frac{1}{\mu_{R_{CC}}R_{CC}^2} + \frac{1}{\mu_R R^2}\right) - 2\frac{p_\varphi^2}{\mu_R R^2} - [\cot\gamma p_\varphi(\cos\varphi\cot\theta p_\varphi + \sin\varphi p_\theta) + (\cos\varphi\cot\theta p_\varphi + \sin\varphi p_\theta)\cot\gamma p_\varphi]/\mu_R R^2 \quad (13)$$

with the following volume element:

$$dV = dR_H\, dR\, dR_{CC}\, d\gamma\, d\varphi \sin\theta\, d\theta \quad (14)$$

If we keep only three degrees of freedom ($\varphi = \pi$) and change the volume element $dV = dR_H\, dR\, dR_{CC}\, d\gamma\, d\varphi\, d\theta$, we obtain the operator eq 1, which is also the well-known diatom−diatom operator for the CCRhH subsystem in which the terms involving p_φ have been eliminated (planar approximation).

The approach presented in this appendix allows one to envision how to improve the operator for the dynamics in the future. Starting from eq 10, it is possible to directly obtain the operator if more degrees of freedom are taken into account, for instance, the third spherical coordinate φ of $\overrightarrow{RhH}$ corresponding to the out-of-plane motion of this vector and several degrees of freedom in C_2H_4. Another possibility to improve the kinetic energy operator is to add the corrections when subjecting the system to rigid constraints. For the two coordinates θ and R_H, such corrections are certainly very small because the H-atom is very light. However, for the angle γ, the corrections coming from freezing the C_2H_4 molecule might play a non-negligible role. They could be added in the future by calculating explicitly the corrections by means of the method described in refs 77, 78. Unfortunately, these corrections are often very involved. However, it should be emphasized that now a code exists that numerically calculates these corrections[79] based on the approach of refs 77 and 78. This code can overcome the problem of the complexity of the constrained operators and could be applied to a system such as the present rhodium complex. On the other hand, the corrections are expected to be quite small for the case of hydrogen motion under consideration. Therefore, we do not include them in the present, first quantal study (beyond 1D) in such systems. u

References and Notes

(1) Brookhart, M.; Green, M.; Wong, L.-L. *Prog. Inorg. Chem.* **1988**, 36, 1.
(2) Brookhart, M.; Lincoln, D.; Volpe, A.; Schmidt, G. *Organometallics* **1989**, *8*, 1212.
(3) Brookhart, M.; Hauptman, E.; Lincoln, D. *J. Am. Chem. Soc.* **1992**, *114*, 10394.
(4) Ittel, S.; Johnson, L.; Brookhart, M. *Chem. Rev.* **2000**, *100*, 1169.
(5) Koga, K.; Morokuma, K. *Chem. Rev.* **1991**, *91*, 823.
(6) Musaev, D.; Morokuma, K. *Adv. Chem. Phys.* **1996**, *95*, 61.
(7) Ziegler, T. *Chem. Rev.* **1991**, *91*, 651.
(8) Salahub, D. R.; Castro, M. E.; Fournier, R.; Calaminici, P.; Godbout, N.; Goursot, A.; Jamorski, C.; Kobayashi, H.; Martinez, A.; Papai, I.; Proynov, E.; Russo, N.; Sirois, S.; Ushio, J.; Vela, A. In *Theoretical and Computational Approaches to Interface Phenomena*; Sellers, H., Golab, J. T., Eds.; Plenum: New York, 1995.
(9) Siegbahn, P. *Adv. Chem. Phys.* **1996**, *93*, 333.
(10) Dedieu, A., Ed. *Transition Metal Hydrides*; Wiley: New York, 1992.
(11) v. Leeuwen, P., v. Lenthe, J., Morokuma, K., Eds. *Theoretical Aspects of Homogeneous Catalysts: Applications of Ab Initio Molecular Orbital Theory*; Kluwer Academic: Dordrecht, The Netherlands, 1994.
(12) Yoshida, S.; Sakaki, S.; Kobayashi, H. *Electronic Processes in Catalysis*; Wiley: New York, 1992.
(13) Senn, H.; Blöchel, P.; Togni, A. *J. Am. Chem. Soc.* **2000**, *122*, 4098.
(14) Meier, R.; v. Doremaele, G.; Ialori, S.; Buda, F. *J. Am. Chem. Soc.* **1994**, *116*, 7274.
(15) Miller, W.; Schwartz, S.; Tromp, J. *J. Chem. Phys.* **1983**, *79*, 4889.
(16) Manthe, U. *J. Theor. Comput. Chem.* **2002**, *1*, 153.
(17) Bittner, M.; Köppel, H. *J. Phys. Chem.* **2004**, *108*, 11116.
(18) Fukui, K.; Sato, S.; Fujimoto, H. *J. Am. Chem. Soc.* **1975**, *97*, 1.
(19) Fukui, K. *Acc. Chem. Res.* **1981**, *14*, 363.
(20) Gonzalez, C.; Schlegel, H. *J. Chem. Phys.* **1989**, *90*, 2154.
(21) Gonzalez, C.; Schlegel, H. *J. Phys. Chem.* **1990**, *94*, 5523.
(22) Kulander, K. *Time-Dependent Methods for Quantum Dynamics*; North-Holland: New York, 1991.
(23) Zhang, J. *Theory and Application of Quantum Molecular Dynamics*; World Scientific: River Edge, NJ, 1999.
(24) Schork, R.; Köppel, H. *J. Chem. Phys.* **2001**, *115*, 7907.
(25) Mahapatra, S.; Köppel, H.; Cederbaum, L. *J. Phys. Chem.* **2001**, *105*, 2321.
(26) Neumark, D. *Annu. Rev. Phys. Chem.* **1992**, *43*, 153.
(27) Neumark, D. *Phys. Chem. Chem. Phys.* **2005**, *7*, 433.
(28) Zewail, A. *Femtochemistry*; World Scientific: New York, 1994.

(29) Manz, J., Wöste, L., Eds. *Femtosecond Chemistry*; Verlag Chemie: New York, 1995.
(30) Becke, A. *J. Chem. Phys.* **1993**, *98*, 1372.
(31) Becke, A. *J. Chem. Phys.* **1993**, *98*, 5648.
(32) Becke, A. *Phys. Rev. A* **1988**, *38*, 3098.
(33) Perdew, J. *Phys. Rev. B* **1986**, *33*, 8822.
(34) Møller, C.; Plesset, M. *Phys. Rev.* **1934**, *46*, 618.
(35) Pople, J.; Binkley, J.; Seeger, R. *Int. J. Quantum Chem. Symp.* **1976**, *10*, 1.
(36) Krishnan, R.; Pople, J. *Int. J. Quantum Chem. Symp.* **1978**, *14*, 91.
(37) Cizek, J. *Adv. Chem. Phys.* **1969**, *14*, 35.
(38) Purvis, G.; Bartlett, R. *J. Chem. Phys.* **1982**, *76*, 1910.
(39) Scuseria, G.; Janssen, C.; Schaefer, H. *J. Chem. Phys.* **1988**, *89*, 7382.
(40) Frisch, M. J.; Trucks, G. W.; Schlegel, H. B.; Scuseria, G. E.; Robb, M. A.; Cheeseman, J. R.; Montgomery, J. A., Jr.; Vreven, T.; Kudin, K. N.; Burant, J. C.; Millam, J. M.; Iyengar, S. S.; Tomasi, J.; Barone, V.; Mennucci, B.; Cossi, M.; Scalmani, G.; Rega, N.; Petersson, G. A.; Nakatsuji, H.; Hada, M.; Ehara, M.; Toyota, K.; Fukuda, R.; Hasegawa, J.; Ishida, M.; Nakajima, T.; Honda, Y.; Kitao, O.; Nakai, H.; Klene, M.; Li, X.; Knox, J. E.; Hratchian, H. P.; Cross, J. B.; Bakken, V.; Adamo, C.; Jaramillo, J.; Gomperts, R.; Stratmann, R. E.; Yazyev, O.; Austin, A. J.; Cammi, R.; Pomelli, C.; Ochterski, J. W.; Ayala, P. Y.; Morokuma, K.; Voth, G. A.; Salvador, P.; Dannenberg, J. J.; Zakrzewski, V. G.; Dapprich, S.; Daniels, A. D.; Strain, M. C.; Farkas, O.; Malick, D. K.; Rabuck, A. D.; Raghavachari, K.; Foresman, J. B.; Ortiz, J. V.; Cui, Q.; Baboul, A. G.; Clifford, S.; Cioslowski, J.; Stefanov, B. B.; Liu, G.; Liashenko, A.; Piskorz, P.; Komaromi, I.; Martin, R. L.; Fox, D. J.; Keith, T.; Al-Laham, M. A.; Peng, C. Y.; Nanayakkara, A.; Challacombe, M.; Gill, P. M. W.; Johnson, B.; Chen, W.; Wong, M. W.; Gonzalez, C.; Pople, J. A. *Gaussian 03*, revision C.02; Gaussian, Inc.: Wallingford, CT, 2003.
(41) Dunning, T.; Hay, P. In *Modern Theoretical Chemistry*; Schaefer, H., Ed.; Plenum: New York, 1976; Vol. 3.
(42) Ditchfield, R.; Hehre, W.; Pople, J. *J. Chem. Phys.* **1971**, *54*, 724.
(43) Hehre, W.; Ditchfield, R.; Pople, J. *J. Chem. Phys.* **1972**, *56*, 2257.
(44) Hariharan, P.; Pople, J. *Mol. Phys.* **1974**, *27*, 209.
(45) JanVerspechtMultiDim. Verspecht, J. www.janverspecht.com, 2004.
(46) Mladenović, M. *J. Chem. Phys.* **2000**, *112*, 1070.
(47) Sibert, E.; Mayrhofer, R. *J. Chem. Phys.* **1993**, *99*, 937.
(48) Liu, L.; Muckermann, J. *J. Chem. Phys.* **1997**, *107*, 3402.
(49) Kozin, I.; Law, M. *J. Chem. Phys.* **2005**, *122*, 064309.
(50) Arnoldi, W. *Q. Appl. Math.* **1951**, *9*, 17.
(51) Saad, Y. *Lin. Alg. Appl.* **1980**, *24*, 269.
(52) Balakrishnan, N.; Kalyanaraman, C.; Sathyamurthy, N. *Phys. Rep.* **1997**, *280*, 79.
(53) Kosloff, R. In *Dynamics of Molecules and Chemical Reactions*; Wyatt, R., Zhang, J., Eds.; Marcel Dekker: New York, 1996, p 185.
(54) Sorensen, H.; Burrus, C.; Heideman, M. *Fast Fourier Transform Database*; PWS Publishing: Boston, 1995.
(55) McClellan, J.; Rader, C. *Number Theory in Digital Signal Processing*; Prentice Hall: New York, 1979.
(56) Nussbaumer, H. *Fast Fourier Transform and Convolution Algorithms*; Springer: New York, 1982.
(57) Neuhauser, D.; Baer, M. *J. Chem. Phys.* **1989**, *90*, 4351.
(58) Vibók, Á.; Balint-Kurti, G. G. *J. Chem. Phys.* **1992**, *96*, 7615.
(59) Vibók, Á.; Balint-Kurti, G. *J. Phys. Chem.* **1992**, *96*, 8712.
(60) Riss, U.; Meyer, H.-D. *J. Chem. Phys.* **1996**, *105*, 1409.
(61) Schinke, R. *Photodissociation Dynamics*; Cambridge University Press: New York, 1993.
(62) Neuhauser, D. *J. Chem. Phys.* **1990**, *93*, 2611.
(63) Neuhauser, D. *J. Chem. Phys.* **1993**, *100*, 5076.
(64) Wall, M.; Neuhauser, D. *J. Chem. Phys.* **1995**, *102*, 8011.
(65) Mandelshtam, V.; Taylor, H. *J. Chem. Phys.* **1997**, *107*, 6756.
(66) Feit, M.; Fleck, J.; Steiger, A. *J. Comput. Phys.* **1982**, *47*, 412.
(67) Sadeghi, R.; Skodje, R. *J. Chem. Phys.* **1993**, *99*, 5126.
(68) Baumert, T.; Brixner, T.; Seyfried, V.; Strehle, M.; Gerber, G. *Appl. Phys. B* **1997**, *65*, 779.
(69) Assion, A.; Baumert, T.; Bergt, M.; Brixner, T.; Kiefer, B.; Seyfried, V.; Strehle, M.; Gerber, G. *Science* **1998**, *282*, 919.
(70) Rice, S.; Zhao, M. *Optical Control of Molecular Dynamics*; Wiley: New York, 2000.
(71) Shapiro, M.; Brumer, P. *Principles of the Quantum Control of Molecular Processes*; Wiley: New York, 2003.
(72) Gatti, F.; Iung, C.; Menou, M.; Justum, Y.; Nauts, A.; Chapuisat, X. *J. Chem. Phys.* **1998**, *108*, 8804.
(73) Gatti, F.; Iung, C.; Menou, M.; Chapuisat, X. *J. Chem. Phys.* **1998**, *108*, 8821.
(74) Gatti, F. *J. Chem. Phys.* **1999**, *111*, 7225.
(75) Mladenović, M. *J. Chem. Phys.* **2000**, *112*, 1070−1081.
(76) Brocks, G.; van der Avoird, A.; Sutcliffe, B. T.; Tennyson, J. *Mol. Phys.* **1983**, *50*, 1025.
(77) Nauts, A.; Chapuisat, X. *Chem. Phys. Lett.* **1987**, *136*, 164.
(78) Gatti, F.; Justum, Y.; Menou, M.; Nauts, A.; Chapuisat, X. *J. Mol. Spectrosc.* **1997**, *373*, 403.
(79) Lauvergnat, D.; Nauts, A. *J. Chem. Phys.* **2002**, *116*, 8560.
(80) Gatti, F.; Munoz, C.; Iung, C. *J. Chem. Phys.* **2001**, *114*, 8275.
(81) Bramley, M. J.; Tromp, J. W.; Carrington, T., Jr.; Corey, R. C. *J. Chem. Phys.* **1994**, *100*, 6175.